Contemporary Mathematics
http://ojs.wiserpub.com/index.php/CM/

Research Article

Heat and Mass Transfer Analysis of Chemically Reactive Powell-Eyring Nanofluid Flow Over a Wedge: A Numerical Approach

Pooja Agarwal[1], Reema Jain[1*], K. Loganathan[1], R. Udhayakumar[2]

[1]Department of Mathematics and Statistics, Manipal University Jaipur, Jaipur-303007, Rajasthan, India
[2]Department of Mathematics, School of Advanced Sciences, Vellore Institute of Technology, Vellore-632014, Tamilnadu, India
E-mail: reemajain197@gmail.com

Received: 26 April 2024; **Revised:** 27 June 2024; **Accepted:** 6 August 2024

Abstract: The present study describes the effects of different parameters on heat and mass transfer phenomena in fluid flow across a wedge. A non-Newtonian chemically reactive Powell-Eyring nanofluid model is considered for analysis. The governing equations for the boundary layer regime are derived by applying the principles of mass, momentum, and energy conservation. Using similarity transformation, the partial differential equations (PDEs), with boundary conditions are converted into ordinary differential equations (ODEs). With prescribed boundary conditions in the free stream and at the wall, these equations are simplified into an ordinary differential equations system. This simplification is attained using appropriate scaling of similarity transformations which produce a number of important dimensionless control parameters. The computational solution to the nonlinear coupled boundary value problem is obtained using the bvp4c numerical tool in MATLAB. The effects of the various physical parameters on the energy, velocity and mass profiles are investigated through graphs and tables. Also, Nusselt number, skin friction coefficient, and Sherwood number are explored. Validation with previous studies is included.

***Keywords*:** Powell-Eyring fluid model, nanofluid, chemical reaction, radiation, Magneto hydro dynamics (MHD), bvp4c

MSC: 76W05, 80A19

Nomenclature

Symbol

C_p	Specific heat [$J \cdot kg^{-1} \cdot K^{-1}$]
C	Nanoparticles concentration [$kg \cdot m^{-3}$]
q_r	Radiative heat flux [$W \cdot m^{-2}$]
D_B	Brownian diffusivity coefficient [$m^2 s^{-1}$]
D_T	Thermophoretic diffusion coefficient [$m^2 s^{-1}$]
α	Thermal diffusivity [$m^2 s^{-1}$]
ρ	Fluid density [$kg \cdot m^{-3}$]
μ	Dynamic viscosity [$kg \cdot m^{-1} s^{-1}$]
θ	Kinematic viscosity of fluid [$m^2 s^{-1}$]

DOI: https://doi.org/10.37256/cm.5320244826

ρ_f	Nanofluid density [kg·m^{-3}]
ρ_p	Nanoparticles density [kg·m^{-3}]
T	Temperature [K]
N_b	Brownian motion coefficient
N_t	Thermophoresis parameter
Rd	Radiation parameter
E_c	Eckert number
P_r	Prandtl number
M	Hartmann number
L_e	Lewis number
λ_1	Powell-Eyring material constant
ε	Powell-Eyring parameter
K_1	Chemical reaction parameter
G_c	Mass Grashof number
G_r	Thermal Grashof number
δ	Source/Sink parameter
η	Similarity transformation parameter
φ	Nondimensional concentration
θ	Nondimensional temperature
τ	Dimensionless heat capacity ratio

Subscripts

w	Fluid condition at wall
∞	Fluid condition at infinity

1. Introduction

The significance of non-Newtonian fluid flow in engineering and industry has drawn a lot of attention in recent years. Non-Newtonian fluids with heat and mass transfer are widely used in the processing of food, making paper, and lubricating processes. Therefore, researchers have developed a variety of non-Newtonian fluid models like Casson, Maxwell, Sisko, Jeffrey, Powell Eyring, Williamson. Recently, many researchers have put their focus on Powell-Eyring fluid model because of its vital function in numerous scientific and technological domains. Krishna et al. [1] examined the unstable flow of a Powell-Eyring fluid via an inclined stretched sheet. Akbar [2] has quoted many applications of Powell-Eyring model. Gireesha et al. [3] investigated the nano particle behavior in Powell-Eyring fluid flow in three dimensions and got significant results. Shuguang et al. [4] explored the thermal outcomes of Eyring Powell material with decomposition of dusty particles. This family of boundary layer flows is associated with the two-dimensional wedge conFigureuration. Several chemical engineering systems include non-Newtonian flows from wedge bodies which have been described in detail. Kandasamy et al. [5] examined the effects of viscosity and thermophoresis on MHD flow through a porous wedge. Later, the effects of viscosity on MHD convective flow over a non-isothermal wedge, which varies with temperature, were demonstrated by Pal et al. [6]. Many researchers [7-10] carried out their studies considering the flow across moving wedge and derived significant results.

"Enhancement of heat transfer is essential in improving performances and compactness of electronic devices. Usual cooling agents (water, oil, etc.) have relatively small thermal conductivities, and therefore heat transfer is not very efficient. Thus, to augment thermal characteristics very small size particles (nanoparticles) were added to fluids forming the so-called nanofluids. These suspensions of nanoparticles in fluids have physical and chemical properties depending on the concentration and the shape of particles. It is observed that adding a little amount of nanoparticles to a base fluid increases the thermal conductivity of the fluid significantly". Macha et al. [11] examined the effect of buoyant forces on boundary layer flow of a viscoelastic nanofluid across a wedge. The fluid properties of the nanofluids themselves influence their flow across a wedge-shaped slip surface, as pointed out by Das et al. [12]. The radiated magnetized flow of Maxwell nanoliquid

over stretching surface with Soret and Dufour effects was explained by Shuguang et al. [13]. Khan et al. [14] applied Cattaneo-Christov heat and mass flux theory in the flow of Maxwell nanofluid and gyrotactic microorganisms towards a spinning disk. Numerous branches of science and engineering can benefit from an understanding of convective flow with heat and mass transfer under the influence of magnetic field and chemical reactions. This phenomenon is significant for the nuclear reactor cooling process, the chemical and petroleum industries, and packed-bed catalytic reactors. Madhu et al. [15] highlighted the heat and mass in Power-law nanofluid. Hayat et al. [16-18] examined the various phenomena of flow considering Powell-Eyring model with different boundary conditions. The MHD Falker-Skan fluid flow was explained by Ghiasi et al. [19]. Peristaltic transport of a Ree-Eyring fluid with heat transmission was explained by Shuguang et al. [20]. Pantokratoras et al. [21] investigated the Falkner-Skan flow with variable viscosity and nonlinear thermal radiation. Furthermore, Hamid et al. [22] computed numerical results for heat transfer in Williamson fluid flow driven by wedge-geometry. Eyring-Powell nanofluid flow across a wedge with thermal radiation was investigated by Raju et al. [23]. Analysis of transport processes and their interaction with chemical reaction has the greatest contributions to many areas of chemical science. The effect of chemical reaction on different geometry of the problem has been investigated by many authors. Das et al. [24] studied the effect of mass transfer flow past an impulsively started infinite vertical plate with heat flux and chemical reaction. Dadhich et al. [25] elaborated the heat and mass transmission in Magneto-Mixed Convective Sisko Nanofluid over a Wedge with Viscous Dissipation. Also, Agarwal et al. [26] extended the study of entropy generation chemically reactive bioconvective Powell-Eyring nanofluid over a riga plate.

From above cited literature, it is evident that no investigation has been carried out to examine the heat and mass transfer analysis of chemically reactive Powell-Eyring nanofluid flow over a wedge. Boundary layer flow over a wedge has become a trending subject in fluid mechanics nowadays due to its thermal engineering applications, for example, thermal insulation heat exchangers, geothermal systems, crude oil extraction, the storage of nuclear waste, etc. So, in the current study an attempt is made to bridge this gap. In this analysis, the governing equations for the boundary layer regime are derived by applying the principles of mass, momentum, and energy conservation. Using similarity transformation, the partial differential equations (PDEs), with boundary conditions are converted into ordinary differential equations (ODEs). With prescribed boundary conditions in the free stream and at the wall, these equations are simplified into an ordinary differential equations system. Numerical simulation is obtained using bvp4c solver in MATLAB. The effects of the various physical parameters on the energy, velocity and mass profiles are investigated through graphs and tables. Also, Nusselt number, skin friction coefficient, and Sherwood number are explored. Validation with previous studies is included.

2. Mathematical formulation

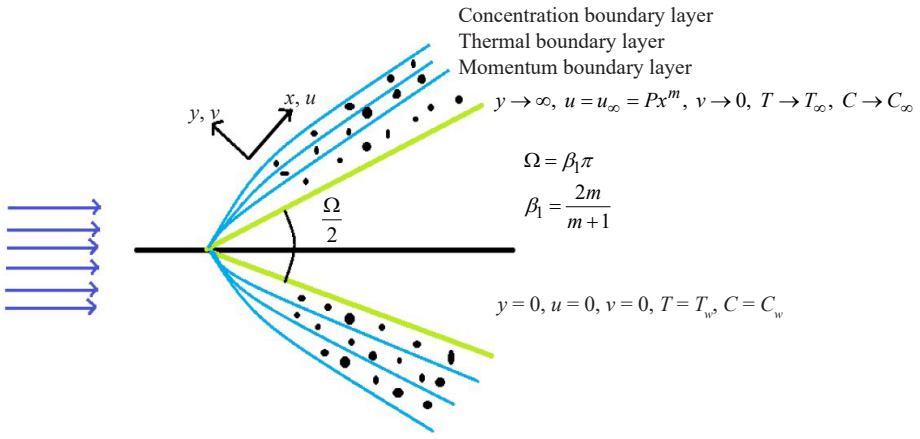

Figure 1. Schematic diagram of current analysis

The regime under consideration comprises steady, incompressible, two-dimensional mixed convective flow of the Powell Eyring nanofluid over a wedge. It is assumed that velocity of the possible flow away from boundary layer is u_{∞}. The temperature T_w and concentration at the wedge are fixed and higher than the ambient concentration C_w and temperature (C_∞, T_∞), respectively. The physical model is depicted in Figure 1.

The expression of the Cauchy stress tensor τ for Powell-Eyring fluid is given by

$$\tau = \mu\nabla V + \frac{1}{\beta_1}\sinh^{-1}\left(\frac{1}{c}\nabla V\right), \tag{1}$$

where τ is shear stress, μ is the dynamic viscosity, V is the fluid velocity, β_1 and c are the fluid parameters of the Powell-Eyring model. The second order approximation for $\sinh^{-1}\left(\frac{1}{c}\nabla V\right)$ is as follows:

$$\sinh^{-1}\left(\frac{1}{c}\nabla V\right) \cong \frac{1}{c}\nabla V - \frac{1}{6}\left(\frac{1}{c}\nabla V\right)^3;\ \left|\frac{1}{c}\nabla V\right| \ll 1. \tag{2}$$

Taking the assumptions stated above into account, the continuity, momentum, energy and mass equations [27] are given by:

$$\frac{\partial u}{\partial x} + \frac{\partial v}{\partial y} = 0, \tag{3}$$

$$u\frac{\partial u}{\partial x} + v\frac{\partial u}{\partial y} = \left(\vartheta + \frac{1}{\rho\beta_1 c}\right)\frac{\partial^2 u}{\partial y^2} - \frac{1}{2\rho\beta_1 c^2}\left(\frac{\partial u}{\partial y}\right)^2\frac{\partial^2 u}{\partial y^2} - \frac{\sigma B_0^2}{\rho}u + g\beta\left(T - T_\infty\right)\sin\left(\frac{\Omega}{2}\right) + g\beta^*\left(C - C_\infty\right)\sin\left(\frac{\Omega}{2}\right), \tag{4}$$

$$u\frac{\partial T}{\partial x} + v\frac{\partial T}{\partial y} = \frac{k}{\left(\rho C_p\right)_f}\frac{\partial^2 T}{\partial y^2} - \frac{1}{\left(\rho C_p\right)_f}\frac{\partial q_r}{\partial y} + \frac{\sigma B_0^2}{\left(\rho C_p\right)_f}u^2 + \frac{\mu}{\left(\rho C_p\right)_f}\left(\frac{\partial u}{\partial y}\right)^2 + \frac{Q}{\left(\rho C_p\right)_f}\left(T - T_\infty\right) + \frac{\left(\rho C_p\right)_p}{\left(\rho C_p\right)_f}\times$$

$$\left[D_B\frac{\partial C}{\partial y}\frac{\partial T}{\partial y} + \frac{D_T}{T_\infty}\left(\frac{\partial T}{\partial y}\right)^2\right], \tag{5}$$

$$u\frac{\partial C}{\partial x} + v\frac{\partial C}{\partial y} = \frac{D_T}{T_\infty}\frac{\partial^2 T}{\partial y^2} + D_B\frac{\partial^2 C}{\partial y^2} - k_1\left(C - C_\infty\right). \tag{6}$$

The boundary conditions prescribed at the wall and the edge of the boundary layer are:

$$u = 0,\ v = 0,\ T = T_w,\ C = C_w \text{ at } y = 0,\ u = u_\infty = Px^m,\ v \to 0,\ T \to T_\infty,\ C \to C_\infty \text{ as } y \to \infty. \tag{7}$$

Here u and v are the velocity components in x and y directions respectively, T and C are the temperature and concentration variables resp., B_0 is the intensity of magnetic field, μ is the fluid viscosity, ρ is the fluid density, k is the thermal conductivity, β is the thermal expansion coefficient β^* is the solutal expansion coefficient, Q is the heat source, g is the gravitational acceleration, σ is the electrical conductivity, k_1 is the chemical reaction rate on the species concentration, Ω wedge angle parameter, β_1 and c are the fluid characteristics (Powell Eyring model). Free stream velocity is $u_\infty = Px^m$ where $m = \frac{\beta_2}{2-\beta_2}$ is the Hartree pressure gradient which corresponds to $\beta_2 = \frac{\Omega}{\pi}$ for total wedge angle Ω and P is a positive number.

To reduce the set of partial differential equations to ordinary differential equations, the following similarity

transformations are used [28, 29]:

$$\eta = y\left(\frac{u_\infty (m+1)}{2\vartheta x}\right)^{1/2},\ \Psi(x,y) = \left(\frac{2\vartheta x u_\infty}{m+1}\right)^{1/2} f(\eta),\ \theta(\eta) = \frac{T-T_\infty}{T_w - T_\infty},\ \phi(\eta) = \frac{C-C_\infty}{C_W - C_\infty},\ u = u_\infty f'(\eta),$$

$$v = -\left(\frac{\vartheta u_\infty}{2(m+1)x}\right)^{1/2}\left[f + \eta f'\right], \tag{8}$$

where a prime denotes the differentiation with respect to η.

Incorporating the above scaling variables (8) into equations (4) to (7), the following nonlinear ordinary differential equations are emerged:

$$\left(\frac{m+1}{2}\right)(1+\varepsilon)f''' + ff'' - \lambda_1 \varepsilon (m+1) f''' - Mf' + \left(G_r\theta + G_c\phi\right)\sin\left(\frac{\Omega}{2}\right) = 0, \tag{9}$$

$$(m+1)\left(1+\frac{4}{3}Rd\right)\theta'' + P_r f\phi' + (m+1)\left(P_r N_b \theta'\phi' + P_r N_t \theta'^2\right) + \delta P_r \theta + MP_r E_c f'^2 + P_r E_c f''^2 = 0, \tag{10}$$

$$(m+1)\phi'' + (m+1)\frac{N_t}{N_b}\theta'' - L_e K_1 \phi + L_e f\phi' = 0 \tag{11}$$

The dimensionless boundary conditions are:

$$f' = 0,\ f = 0,\ \theta = 1,\ \phi = 1 \text{ at } \eta = 0, \tag{12}$$

$$f' = 1,\ \theta = 0,\ \phi = 0,\ f = 0 \text{ as } \eta \to \infty. \tag{13}$$

Following are the governing parameters involved in the above equations (9-11):

$$M = \frac{\sigma B_0^2}{\rho u_\infty x},\ \varepsilon = \frac{1}{\rho\vartheta\beta_1 c},\ \lambda_1 = \frac{u_0^3}{xvc^2}\left(\frac{m+1}{2}\right),\ E_c = \frac{2x^2u_\infty^2}{\left(\rho C_p\right)_f (T_w - T_\infty)},\ P_r = \frac{\vartheta}{\alpha},\ \alpha = \frac{k}{\left(\rho C_p\right)_f},\ Rd = \frac{4\sigma^* T_\infty^3}{kk^*},$$

$$N_b = \frac{\left(\rho c_p\right)_p D_B (C_w - C_\infty)}{\left(\rho c_p\right)_f \vartheta},\ N_t = \frac{D_T (T_w - T_\infty)}{T_\infty \vartheta},\ L_e = \frac{\vartheta}{D_B},\ \delta = \frac{2xQ}{\left(\rho c_p\right)_f \alpha},\ K_1 = \frac{2k_1 x}{u_\infty},\ G_n = \frac{g\beta(T_w - T_\infty)x^3}{\vartheta^2},$$

$$G_c = \frac{g\beta^*(C_w - C_\infty)x^3}{\vartheta^2}.$$

3. Coefficients of heat and mass transport

The pertinent quantities of engineering interest like Skin friction coefficient (C_f), local Nusselt number $\left(N_{u_x}\right)$ and local Sherwood number (Sh_x) are defined as follows:

$C_f = \frac{\tau_w}{\rho u_\infty^2}$; where wall shear stress $\tau_w = \mu\left(\frac{\partial u}{\partial y}\right)_{y=0}$,

$N_{u_x} = \left(\frac{xq_w}{k\left(T_w - T_\infty\right)} \right)_{y=0}$; where the local heat flux $q_w = -k\left(\frac{\partial T}{\partial y}\right)_{y=0}$,

$Sh_x = \left(\frac{xq_m}{D_B\left(C_w - C_\infty\right)} \right)_{y=0}$; where the local mass flux $q_m = -D_B\left(\frac{\partial C}{\partial y}\right)_{y=0}$.

After applying similarity transformation, the following expressions describe local skin friction, heat transfer rate, and mass transfer rate:

$$R_{e_x}^{\frac{1}{2}} C_f = \left[(1+\varepsilon) f''(0) - \frac{\lambda_1 \varepsilon}{3} f'''(0) \right], \tag{14}$$

$$N_{u_x} \left(R_{e_x}\right)^{\frac{-1}{2}} = -\left(1 + \frac{4Rd}{3}\right)\theta'(0), \tag{15}$$

$$Sh_x \left(R_{e_x}\right)^{\frac{-1}{2}} = -\phi'(0). \tag{16}$$

4. Solution methodology

An analytical solution of boundary value problem defined by eqns. (7)-(9) is difficult due to the strong coupling, nonlinearity and multi-degree terms. Therefore, the governing equations (7)-(9) and boundary conditions (10, 11) are solved numerically using the bvp4c algorithm in MATLAB. The numerical solution is found using this package by fixing the convergence criteria to 0.000001. The bvp4c solver implements a numerical method called 3-stage Lobatto IIa collocation. This method belongs to the finite difference discretization family of techniques [30]. To use the bvp4c solver, the nonlinear ordinary differential equations and boundary conditions need to be reformulated as first order equations and the basic syntax used is sol = bvp4c (@OdeBVP, @OdeBC, solinit). The "solinit" function contains the initial mesh points and initial guesses at these points. Multiple solutions can be obtained by providing additional initial guesses in the solinit function. The reduced system is formulated as:

$$f = y_1,\ f' = y_2,\ f'' = y_3,\ \theta = y_4,\ \theta' = y_5,\ \phi = y_6,\ \phi' = y_7,$$

$$f''' = y_3' = \frac{My_2 - y_1 y_3 - \left(G_r y_4 + G_c y_6\right)\sin(\Omega/2)}{\left(\frac{m+1}{2}\right)(1+\varepsilon) - \varepsilon\lambda_1(m+1)},$$

$$\theta'' = y_5' = \frac{-P_r y_1 y_7 - (m+1)\left(P_r N_b y_5 y_7 + P_r N_t y_5^2\right) - \delta P_r y_4 - MP_r E_c y_2^2 - P_r E_c y_3^2}{(m+1)\left(1 + \frac{4}{3}Rd\right)},$$

$$\phi'' = y_7' = \frac{L_e K_1 y_6 - L_e y_1 y_7 - \left(\frac{N_t}{N_b}\right)(m+1) y_5'}{(m+1)} \tag{17}$$

The corresponding boundary conditions are:

$$y_1(0)=0,\ y_2(0)=0,\ y_4(0)-1=0,\ y_6(0)-1=0,\ y_2(1)-1=0,\ y_4(1)=0,\ y_6(1)=0. \tag{18}$$

5. Result and discussion

The effect of each pertinent parameter involved in the study on fluid velocity $f'(\eta)$, temperature $\theta(\eta)$ and concentration $\varphi(\eta)$, is highlighted and discussed in this section. Comprehensive results are obtained and are presented in Tables 1-3 and Figures 2-17.

Figures 2-4 portray the effect of Hartmann number M on f', θ and φ profiles. It can be seen from Figure 2, the fluid velocity drops as the value of M increases. It is due to the Lorentz force which is produced by the induced magnetic field and subsequently retards the motion. In the fluid flow regime, the resistive force generates extra heat as M increases, hence the boost in temperature and concentration is observed. Figures 5-6 depict that there is a negative correlation between P_r and fluid velocity which is true practically also. Similar behavior is observed for temperature as well. Increasing value of P_r enhances the viscous force and reduces the thermal conductance of the fluid, resulting a deduction in the velocity and temperature; the opposite behavior is observed in the concentration profile. As P_r increases, thermal conductivity of fluid decreases, causing a decrease in thermal boundary layer thickness, and source term also contributes to the rise of concentration which can be observed from Figure 7. The impact of chemical reaction parameter K_1 is discussed by Figures 8-9. It is observed that an increase in K_1 decreases the concentration, whereas the temperature of the fluid increases. It is due to the heat produced by the chemical reaction taking place in the fluid flow domain. Figures 10-11 indicate the effect of radiation parameter R_d on temperature and concentration profiles. The increasing values of R_d strengthens the thermal layer which results in an increment in temperature and a reduction in concentration. To analyze the effect of wedge angle on f' and θ, it is pertinent to mention that the Hartree pressure gradient $m=\dfrac{\beta_2}{2-\beta_2}$ corresponds to $\beta_2=\dfrac{\Omega}{\pi}$ for total wedge angle Ω. Figures 12-13 illustrate that as the wedge angle increases, the fluid velocity is enhanced but the temperature diminishes. This is due to the fact that an increase in wedge angle is related to an increase in fluid pressure. As thermophoresis parameters N_t improves, temperature and concentration profiles increase as shown in Figures 14-15. It is due to the movement of particles from a hot surface to cool region. The temperature profile also upgrades when the Brownian motion parameter N_b is increased, as demonstrated in Figure16. Because with the rising values of N_b, the intensity of the movement of the nanoparticles increases which leads to increment in kinetic energy of the particles and hence enhance the temperature field. Figure 17 represents the impact of thermal Grashof number G_r on the velocity profile and a positive correlation can be seen. Since G_r signifies the relative effects of the thermal buoyancy force to the viscous hydrodynamic force in the boundary layer so as anticipated, velocity increases due to the boost in thermal buoyancy force.

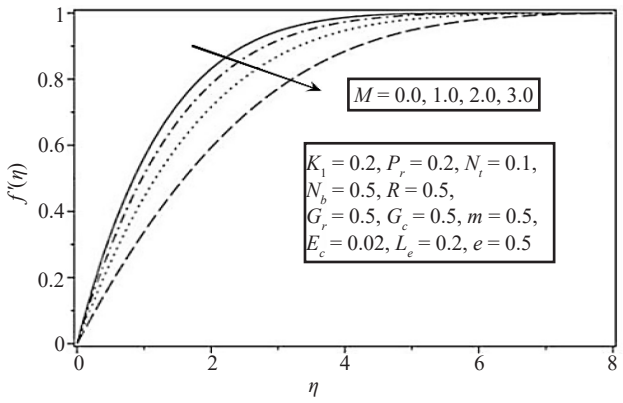

Figure 2. f' vs M

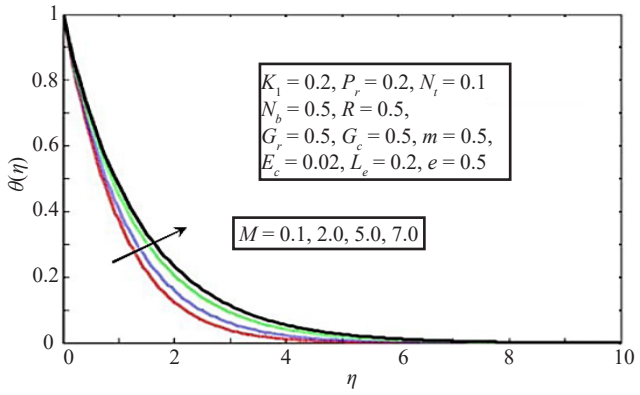

Figure 3. θ vs M

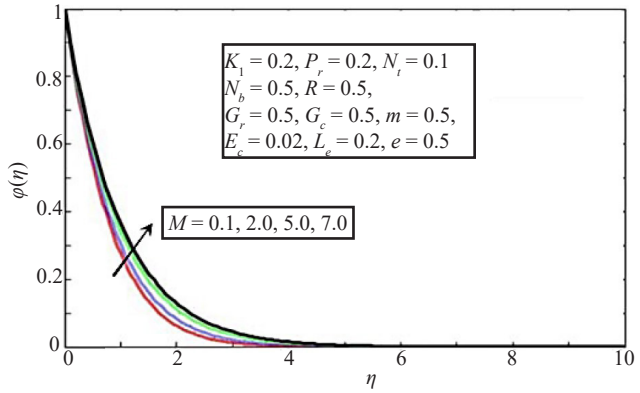

Figure 4. φ vs M

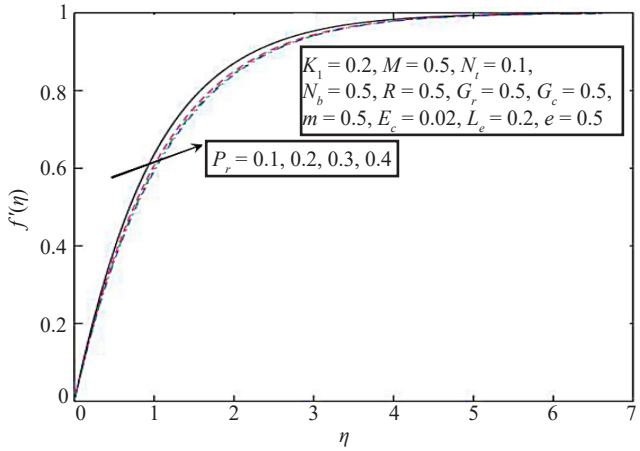

Figure 5. f' vs P_r

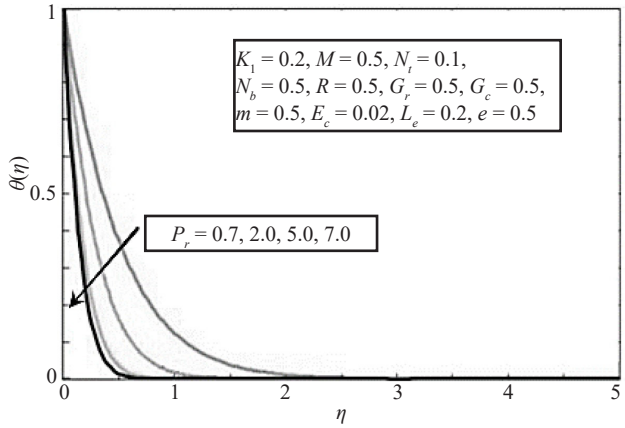

Figure 6. θ vs P_r

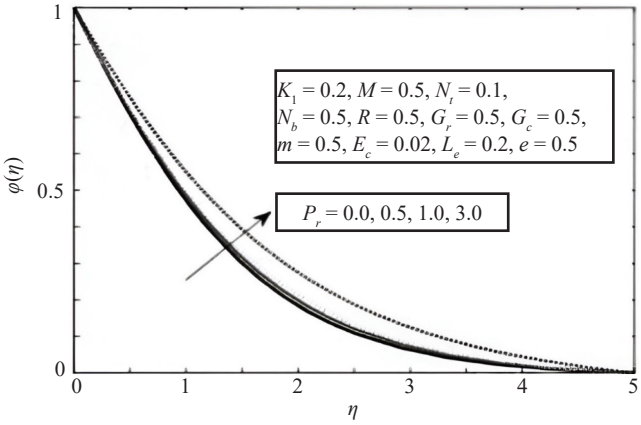

Figure 7. φ vs P_r

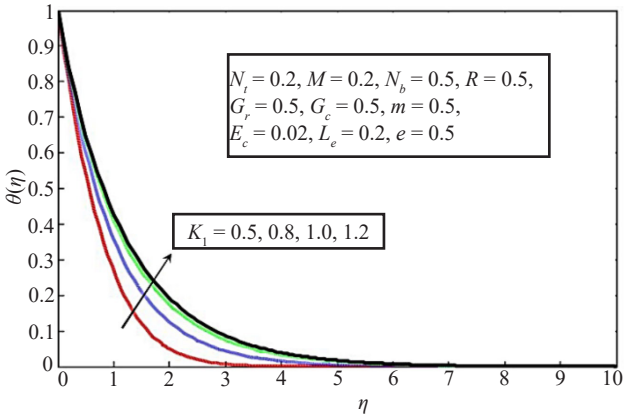

Figure 8. θ vs K_1

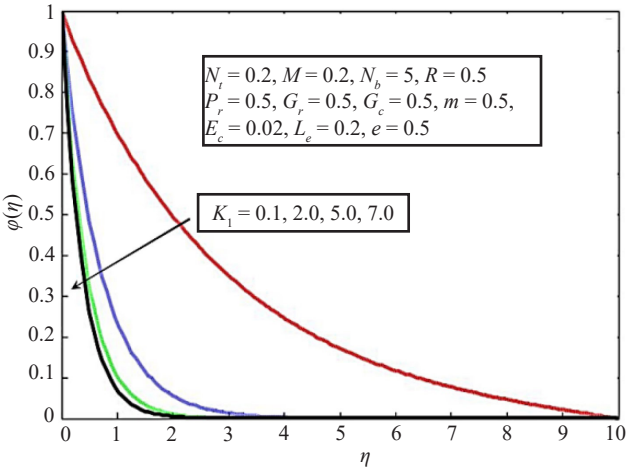

Figure 9. φ vs K_1

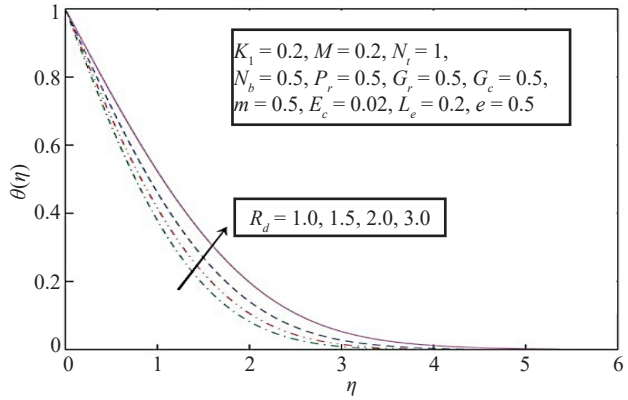

Figure 10. θ vs R_d

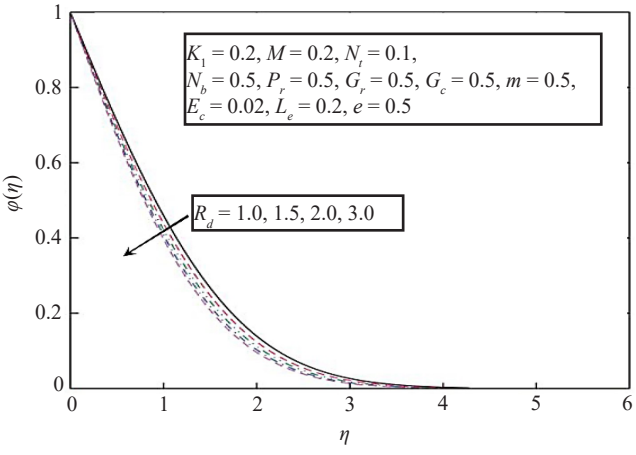

Figure 11. φ vs R_d

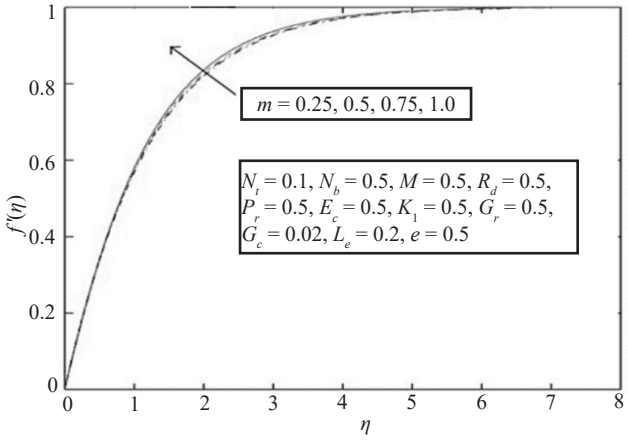

Figure 12. f' vs m

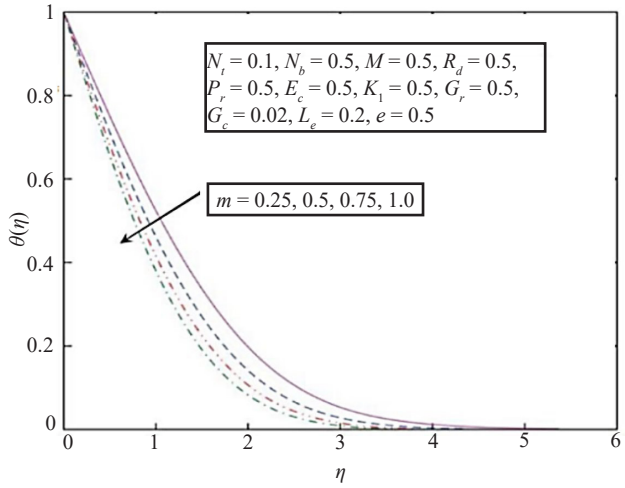

Figure 13. θ vs m

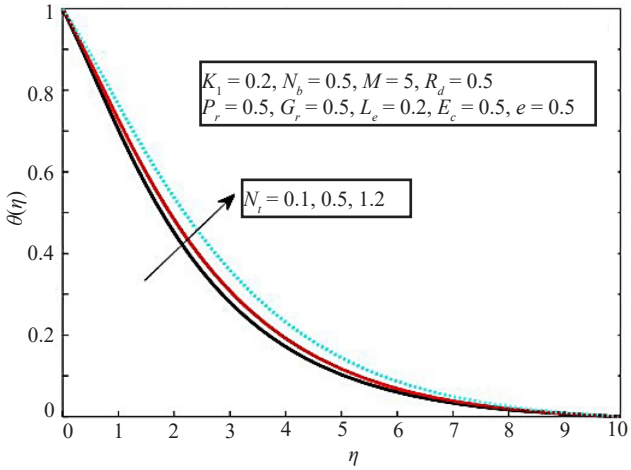

Figure 14. θ vs N_t

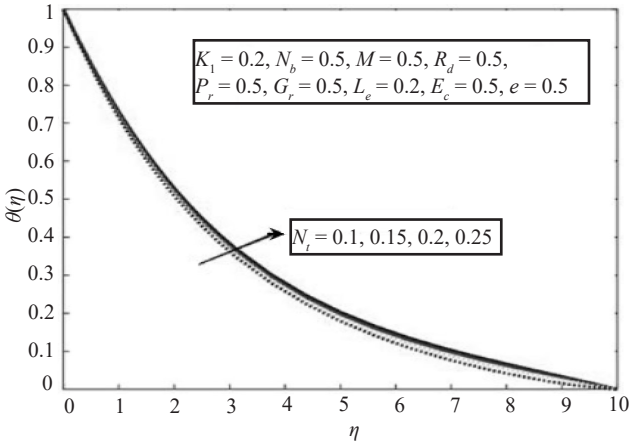

Figure 15. φ *vs* N_t

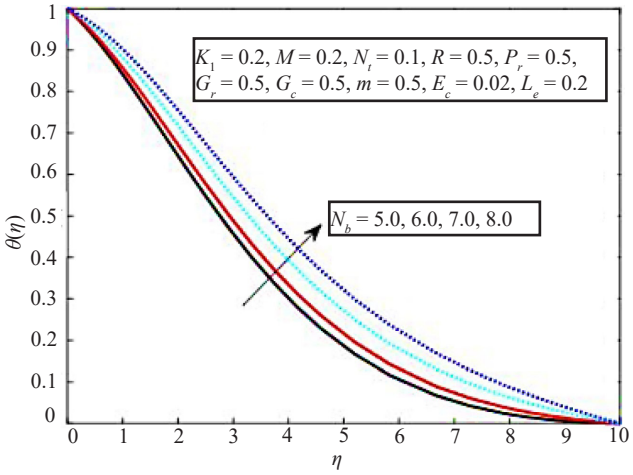

Figure 16. θ vs N_b

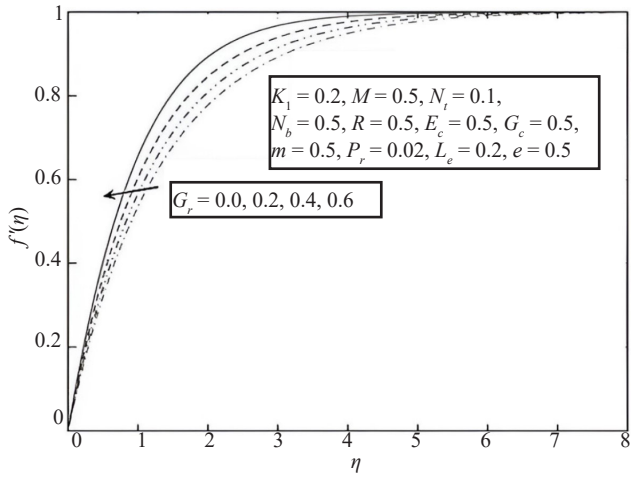

Figure 17. f' vs G_r

The numerical results for the rate of heat transfer are compared with the established results in Table 1 and are found in good agreement with the existing literature which validates the current study also. The impact of Lewis number L_e on $f''(0)$, $-\theta'(0)$ and $-\varphi'(0)$ is indicated in Table 2. It shows that $f''(0)$ declines with increasing L_e, but $-\theta'(0)$ and $-\varphi'(0)$ are reduced. Table 3 illustrates the behavior of skin friction coefficient, local Nusselt number, and local Sherwood number with the change of various physical parameters.

Table 1. The values of P_r for Newtonian fluids when comparing different values of $-\theta'(0)$, $\varepsilon = 0$, $L_\varepsilon = 0$, $M = 0$, $N_t = 0$, $N_b = 0$, $\lambda_1 = 0$, $G_r = 0$, $G_c = 0$, $m = 1$, $K_1 = 0$

P_r	Magyari et al. [26]	Abbas et al. [27]	Present study
1	-0.9547	-0.9551	-0.9555
3	-1.8691	-1.8121	-1.8523
5	-2.5001	-2.5577	-2.5428
10	-3.6604	-3.6868	-3.6876

Table 2. Effects of L_e on (a) $f''(0)$, (b) $-\theta'(0)$, (c) $-\varphi'(0)$ when $\varepsilon = 0.5$, $P_r = 1.5$, $M = 0.1$, $N_t = 0.1$, $N_b = 0.2$, $\lambda_1 = 0.5$, $G_r = 0.5$, $G_c = 0.5$, $m = 0.5$, $K_1 = 0.5$

L_e	$f''(0)$	$-\theta'(0)$	$-\varphi'(0)$
0.1	0.2798	0.7832	-0.1535
2.0	0.0376	0.6258	-1.1111
5.0	0.0611	0.5496	-1.8538
7.0	0.0625	0.4897	-2.2144

Table 3. Variation of $Re_x^{\frac{1}{2}} C_f$, $Nu_x \left(Re_x\right)^{\frac{-1}{2}}$ and $Sh_x \left(Re_x\right)^{\frac{-1}{2}}$ with various physical parameters

Ω	ε	G_r	K_1	M	$Re_x^{\frac{1}{2}} C_f$	$Nu_x \left(Re_x\right)^{\frac{-1}{2}}$	$Sh_x \left(Re_x\right)^{\frac{-1}{2}}$
0					0.7787	0.3584	2.1474
$\frac{\pi}{6}$					1.0625	04897	2.2144
$\frac{\pi}{2}$					2.8429	0.8631	2.0899
	0				0.1039	0.4874	2.2168
	0.2				0.0858	0.4884	2.2157
	0.4				0.0698	0.4893	2.2148
		0			0.6126	0.3640	2.1536
		1.0			0.7691	0.4219	2.2950
		2.0			3.2438	0.6938	2.6329
			0		0.0895	0.5421	1.6564
			0.2		0.0880	0.5179	1.8960
			0.5		0.0858	0.4884	2.2157
				0	0.1879	0.5404	2.2200
				0.5	0.6582	0.3121	2.2024
				1.0	2.2806	0.1476	2.1931

6. Conclusions

In the current study, a mathematical model is developed to carry out the theoretical analysis for heat and mass transfer in MHD flow of the Powell Eyring nanofluid over a wedge in the presence chemical reaction and thermal radiation along with convective surface boundary condition. The major outcomes are summarized as follows:

• The higher values of pressure gradient parameter lead to enhance the fluid velocity and reduce the temperature.

• Increasing values of magnetic field retards the fluid velocity and heat transfer rate.

• Fluid velocity and temperature both are inversely proportional to Prandtl number.

• The velocity of fluid is more pronounced for higher values of thermal Grashof number.

• By increasing the chemical reaction parameter, the temperature goes up, but concentration shows the opposite trend. Same phenomena are observed with increasing values of radiation parameter.

• Fluid temperature boosts with an increase in thermophoresis and Brownian motion parameters.

The present work can be further extended to investigate the effects of inclined magnetic fields, viscous dissipation, and unsteady flow over curved stretching surfaces like cone and riga plate.

Conflict of interest

The authors declare no competing financial interest.

References

[1] Krishna PM, Sandeep N, Reddy JVR, Sugunamma V. Dual solutions for unsteady flow of powell-eyring fluid past an inclined stretching sheet. *Journal of Naval Architecture and Marine Engineering*. 2016; 13(1): 89.

[2] Akbar NS. Application of eyring-powell fluid model in peristalsis with nano particles. *Journal of Computational and Theoretical Nanoscience*. 2015; 12(1): 94-100.

[3] Gireesha BS, Gorla RSR, Mahanthesh B. Unsteady three-dimensional mhd flow of a nano eyring-powell fluid past a convectively heated stretching sheet in the presence of thermal radiation, viscous dissipation and Joule heating. *Journal of the Association of Arab universities for Basic and Applied Sciences*. 2017; 23(1): 75-84.

[4] Shuguang Li, Khan MI, Khan SU, Abdulla S, Mohammad I, Amzad MS. Effectiveness of melting phenomenon in two phase dusty carbon tudes (Nanomaterials) flow of eyring-powell fluid: Heat transfer analysis. *Chinese Journal of Physics*. 2023; 86(11): 160-169.

[5] Kandasamy R, Muhaimin I, Khamis AB. Thermophoresis and variable viscosity effects on mhd mixed convective heat and mass transfer past a porous wedge in the presence of chemical reaction. *Journal of Heat Mass Transfer*. 2009; 45(6): 703-712.

[6] Pal D, Mondal H. Influence of temperature-dependent viscosity and thermal radiation on mhd forced convection over a non-isothermal wedge. *Journal of Applied Mathematics and Computation.* 2009; 212(1): 194-208.

[7] Ishak A, Nazar R, Pop I. Falkner-skan equation for flow past a moving wedge with suction or injection. *Journal of Applied Mathematical Computation*. 2007; 25: 67-83. Available from: https://doi.org/10.1007/BF02832339.

[8] Ishak A, Nazar R, Pop I. Moving wedge and flat plate in a micropolar fluid. *International Journal of Engineering Sciences*. 2006; 44: 1225-1236. Available from: https://doi.org/10.1016/j.ijengsci.2006.08.005.

[9] Hsiao KL. Mhd mixed convection for viscoelastic fluid past a porous wedge. *International Journal of Non-Linear Mechanics*. 2011; 46(1): 1-8.

[10] Mukhopadhyay M, Mondal IC, Chamkha AJ. Casson fluid flow and heat transfer past a symmetric wedge. *Heat Transfer Asian Research*. 2013; 42(8): 665-675.

[11] Macha M, Naikoti K. Boundary layer flow of viscoelastic nanofluid over a wedge in the presence of buoyancy force effects. *Computational Thermal Sciences*. 2018; 9(3): 257-267.

[12] Das K, Acharya N, Kundu PK. Influence of variable fluid properties in nanofluid flow over a wedge with surface slip. *Arabian Journal for Science and Engineering*. 2018; 43: 2119-2131. Available from: https://doi.org/10.1007/s13369-017-2499-x.

[13] Shuguang Li, Imtiaz M, Khan M, Kumar N, Akramova K. Applications of Soret and Dufour effects for Maxwell nanomaterial by convectively heated surface. *Numerical Heat Transfer, Part A: Applications.* 2024; 1-15. Available

from: https://doi.org/10.1080/10407782.2024.2314224.
[14] Khan N, Humphries UW, Kumam W. Dynamic pathways for the bioconvection in thermally activated rotating system. *Biomass Conversion and Biorefinery*. 2024; 14: 8605-8623. Available from: https://doi.org/10.1007/s13399-022-02961-9.
[15] Madhu M, Kishan N. Finite element analysis of heat and mass transfer by mhd mixed convection stagnation-point flow of a non-newtonian power-law nanofluid towards a stretching surface with radiation. *Journal of the Egyptian Mathematical Society*. 2016; 24(3): 458-470.
[16] Hayat T, Waqas M, Khan SM, Alsaedi A. Newtonian heating effect in nanofluid flow by a permeable cylinder. *European Journal of Results in Physics*. 2017; 7: 256-262. Available from: https://doi.org/10.1016/j.rinp.2016.11.047.
[17] Hayat T, Shahzad SA, Waqas M, Alsaedi A. Mixed convection stagnation-point flow of powell-eyring fluid with newtonian heating, thermal radiation, and heat generation/absorption. *Journal of Aerospace Engineering*. 2016; 30(1): 197-222.
[18] Hayat T, Makhdoom S, Awais M, Saleem S, Rashidi MM. Axisymmetric powell-eyring fluid flow with convective boundary conditions: Optimal analysis. *Applied Mathematical and Mechanics*. 2016; 37(7): 919-928.
[19] Ghiasi EK, Saleh R. Nondimensional optimization of magnetohydrodynamics falkner-skan fluid flow. *Journal of Inae Letters*. 2018; 3(3): 143-147.
[20] Shuguang S, Rajashekhar C, Nisar K, Oudina F, Vaidya H, Khan M, et al. Peristaltic transport of a ree-eyring fluid with non-uniform complaint channel: An analysis through varying conditions. *Zamm-Journal of Applied Mathematics and Mechanics*. 2023; 104(2): e202300073. Available from: https://doi.org/10.1002/zamm.202300073.
[21] Pantokratoras A, Fang T. The Falkner-Skan flow with variable viscosity and nonlinear roseland thermal radiation. *Heat Transfer Research*. 2018; 49(6): 569-582.
[22] Hamid A, Khan M. Numerical simulation for heat transfer performance in unsteady flow of Williamson fluid driven by a wedge-geometry. *Results in Physics*. 2018; 9: 479-485. Available from: https://doi.org/10.1016/j.rinp.2018.01.025.
[23] Raju CH, Reddy C, Alyami M, Eldin S, Asogwa K, Dharmaiah V. Mhd eyring-powell nanofluid flow across a wedge with convective and thermal radiation. *Frontiers in Energy Research.* 2022; 10: 1021491. Available from: https://doi.org/10.3389/fenrg.2022.1021491.
[24] Das UN, Deka R, Soundalgekar VM. Effects of mass transfer on flow past an impulsively started infinite vertical plate with constant heat flux and chemical reaction. *Forschung im Ingenieurwesen/Engineering Research*. 1994; 60(10): 284-287.
[25] Dadhich Y, Jain R, Gyeltshen S. Insights of heat and mass transfer in magneto-mixed convective sisko nanofluid over a wedge with viscous dissipation. *Mathematical Problems in Engineering*. 2022; 2022(1): 3091897. Available from: https://doi.org/10.1155/2022/3091897.
[26] Agarwal P, Loganathan K, Jain R. Entropy optimization of chemically reactive bioconvective powell-eyring nanofluid stratified flow over a riga plate: A non-fourier heat and mass flux modelling. *Partial Differential Equations in Applied Mathematics*. 2024; 9: 100616. Available from: https://doi.org/10.1016/j.padiff.2024.100616.
[27] Hayat T, Iqbal Z, Qasim M, Obaidat S. Steady flow of an eyring powell fluid over a moving surface with convective boundary conditional. *International Journal of Heat and Mass Transfer*. 2012; 55(7-8): 1817-1822.
[28] Munir A, Shahzad A, Khan M. Convective flow of Sisko fluid over a wedge with viscous dissipation. *Journal of the Brazilian Society of Mechanical Sciences and Engineering*. 2016; 38(2): 581-587.
[29] Khan M, Shahzad A. Falkner-skan boundary layer flow of a sisko fluid. *Zeitschrift Fur Naturforschung A*. 2014; 67(8-9): 469-478.
[30] Kierzenka J, Shampine LF. A bvp solver that controls residual and error. *Journal of Numerical Analysis, Industrial and Applied Mathematics (JNAIAM)*. 2008; 3(1): 27-41.